

FRONTIER FIELDS CLUSTERS: PROPERTIES OF THE X-RAY-BRIGHT GAS IN THE LARGE-SCALE FILAMENT CROSSING MACS J0717.5+3745

G. A. OGREAN^{1,†}, C. JONES², T. WHALEN³, R. J. VAN WEEREN^{2,‡}, N. WERNER¹, W. FORMAN², T. MROCKOWSKI⁴, ET AL.

¹KIPAC, Stanford University, 452 Lomita Mall, Stanford, CA 94305, USA; gogrean@stanford.edu

²Harvard-Smithsonian Center for Astrophysics, 60 Garden Street, Cambridge, MA 02138, USA;

³University of Maryland, College Park, MD 20742, USA; and

⁴ESO - European Organization for Astronomical Research in the Southern hemisphere, Karl-Schwarzschild-Str. 2, D-85748 Garching b. München, Germany

Submitted to ApJL. Draft version dated August 11, 2016.

ABSTRACT

We present results from deep *Chandra* observations of the large-scale filament extending SE from the massive Frontier Fields cluster MACS J0717.5+3745. The filament was previously found to have a length of ~ 19 Mpc. Within the filament, about 2 Mpc away from the cluster center, there is a galaxy group with a mass of $\sim 7 \times 10^{13} M_{\odot}$ and a temperature of ~ 3 keV. This group is likely infalling for the first time towards the cluster. The filament is brightest in the X-ray in the region between the group and the cluster. Here, the gas is found to have a temperature of $1.58^{+0.51}_{-0.25}$ keV and a density of $\sim 10^{-4} \text{ cm}^{-3}$. The filament density corresponds to a relatively high over-density of ~ 100 relative to the critical density of the Universe, which can be explained by the fact that we are probing only the densest part of the filament. The filament properties are consistent with numerical simulations and with the few other observational results reported to date.

Keywords: Galaxies: clusters: individual: MACS J0717.5+3745 — Galaxies: clusters: intracluster medium — X-rays: galaxies: clusters

1. INTRODUCTION

In the Λ CDM cosmological model, structure in the Universe is organized in a filamentary web in which large-scale cosmic filaments connect virialized massive structures such as clusters and groups of galaxies (e.g., Einasto et al. 1994). Approximately a third of the total baryonic matter is expected from hydrodynamic simulations (e.g. Davé et al. 2001), in the form of low-density gas with temperatures of $10^5 - 10^7$ K—the warm-hot intergalactic medium (WHIM). One of the main signatures of cosmic filaments is soft X-ray emission. However, the low density of the gas within the filaments poses a significant observational challenge, which causes detections to strongly depend on fortuitous alignments of the filaments with our line of sight. As a consequence, there have been only a handful of filament detections, among which are the one in MACS J0717.5+3745 (Ebeling et al. 2004), the one between A222-A223 (Dietrich et al. 2005; Werner et al. 2008), and several in A2744 (Eckert et al. 2015).

Clusters of galaxies grow via the infall of gas and less massive structures along cosmic filaments (e.g., Springel et al. 2006). During infall and subsequent collision with the cluster, less massive structures will be ram-pressure stripped as they fly through the cluster’s denser regions. Consequently, depending on their original density, these structures are either fully destroyed, or their compact cores survive and develop tails in their wakes. An example of the latter scenario is seen in the cluster 1E 0657–

558 (Elvis et al. 1992), in which the collision of a massive cluster with a cluster about 1/10 of its mass (Springel & Farrar 2007; Mastropietro & Burkert 2008) resulted in the famous “bullet” morphology of the less massive structure (Markevitch et al. 2002).

Here, we present results from *Chandra* observations of the merging galaxy cluster MACS J0717.5+3745. MACS J0717.5+3745 ($z = 0.546$; Ebeling et al. 2001, 2007) is one of the most complex merging systems discovered to date, being the site of collisions between four substructures (Ma et al. 2009; Medezinski et al. 2013). The superposition of the dark matter halos of these substructures also makes MACS J0717.5+3745 the largest known gravitational lens (Zitrin et al. 2009; Medezinski et al. 2013; Umetsu et al. 2014, 2016). By analyzing the distribution of galaxies in the cluster region, Ebeling et al. (2004) discovered a large-scale cosmic filament extending SE of MACS J0717.5+3745. Jauzac et al. (2012) found the filament to be ~ 19 Mpc long. Follow-up *Chandra* observations of the intracluster medium (ICM) in the cluster found hot regions with temperatures of ~ 20 keV, remnant cool cores with temperatures of ~ 5 keV, and density and temperature jumps at the interface between the cluster and the SE filament Ma et al. (2009). The authors speculated that the jumps are caused by accretion of gas from the filament onto the cluster. The archival *Chandra* observations also revealed a group of galaxies projected onto the large-scale filament, although this structure is not discussed by Ma et al. (2009). More recently, we have analyzed the thermodynamic properties of the ICM of MACS J0717.5+3745 using deeper *Chandra* observations (van Weeren et al., submitted). In this letter, we present the physical properties of the SE filament connected to MACS J0717.5+3745, and those of

[†] Hubble Fellow

[‡] Clay Fellow

the group seen in the filament. The analysis is based on the same datasets that were used by van Weeren et al., submitted.

In Section 2, we summarize the processing of the *Chandra* datasets. The properties of the group in the filament are discussed in Section 3, while those of the filament are discussed in Section 4. Our conclusions are summarized in Section 5.

Throughout the paper we assume a Λ CDM cosmology with $H_0 = 70 \text{ km s}^{-1} \text{ Mpc}^{-1}$, $\Omega_m = 0.3$, and $\Omega_\Lambda = 0.7$. For these parameters, 1 arcmin at the redshift of MACS J0717.5+3745 ($z = 0.546$) corresponds to a linear distance of approximately 383 kpc.

2. DATA PROCESSING AND BACKGROUND MODELING

Chandra observed MACS J0717.5+3745 four times between Jan 2001 and Dec 2013, for a total of 243 ks. Of the four ObsIDs, two (1655 and 16235) were taken in FAINT mode, while the other two (4200 and 16305) were taken in VFAINT mode. More details about the observation parameters can be found at the [Chandra Data Archive](#).

The ObsIDs were reprocessed to apply the newest calibration files as of Feb 2016 (v4.7.2). Time periods affected by soft protons were removed from the data using the CIAO script *deflare*. ObsID 1655 had residual soft proton flares and we decided to remove it from the spectral analysis. The total clean exposure time after flare filtering was approximately 209 ks (193 ks for the spectral analysis, ignoring ObsID 1655). Point sources were detected in the energy bands 0.5–2 and 2–7 keV using the script *wavdetect*, were visually confirmed, and excluded from the analysis. The instrumental background was subtracted using the epoch-specific stowed background files available in the CalDB. Before subtraction, the instrumental background files were normalized to have the same 10–12 keV count rate as the corresponding source files.

The sky background was modeled as the sum of unabsorbed emission from the Local Hot Bubble, absorbed emission from the Galactic Halo, and absorbed emission from unresolved X-ray sources. The hydrogen column density was fixed to $8.4 \times 10^{20} \text{ cm}^{-2}$, corresponding to the sum of the atomic and molecular hydrogen column densities in the direction of MACS J0717.5+3745⁴ (Kalberla et al. 2005; Willingale et al. 2013). All the foreground components were assumed to have solar metallicities equal to those reported by Feldman (1992).

A more detailed description of the data processing and the background modeling is provided by van Weeren et al., submitted. Our analysis can also be reproduced by the reader by downloading the datasets from the [Chandra Data Archive](#) and running the JUPYTER notebook⁵ available on Github at <https://goo.gl/e8xQD0>.

3. GROUP IN THE FILAMENT

The group of galaxies within the large-scale filament is located a little over 2 Mpc SE of the cluster center, fixed at RA = $07^{\text{h}} 17^{\text{m}} 30.025^{\text{s}}$, Dec = $+37^\circ 45' 18.58''$ for consistency with Jauzac et al. (2012). The small size of the group and its large distance from the cluster implies that it is falling for the first time towards

Table 1

Parameters of the regions used for the spectral analysis. The regions are shown in Figure 2. Uncertainties are quoted at the $\Delta C = 1$ level.

FOREGROUND AND BACKGROUND		
Model Component	Temperature ^a	Normalization ^b
Local Hot Bubble	$0.135^{+0.007}_{-0.008}$	$7.21^{+0.30}_{-0.18} \times 10^{-7}$
Galactic Halo	$0.59^{+0.09}_{-0.08}$	$2.78^{+0.45}_{-0.44} \times 10^{-7}$
Unresolved Background	–	$4.44^{+0.35}_{-0.37} \times 10^{-7}$
Sources ObsID 16235/16305	–	–
Unresolved Background	–	$7.02^{+0.49}_{-0.58} \times 10^{-7}$
Sources ObsID 4200	–	–
LARGE-SCALE FILAMENT		
Model Component	Temperature ^a	Normalization ^b
On Filament	$1.58^{+0.51}_{-0.25}$	$4.00^{+0.56}_{-0.60} \times 10^{-5}$
Off Filament	$11.55^{+9.09}_{-3.95}$	$1.55^{+0.14}_{-0.10} \times 10^{-5}$
GROUP IN THE FILAMENT		
	Temperature ^a	Normalization ^b
	$4.19^{+0.76}_{-0.48}$	$8.40^{+0.52}_{-0.53} \times 10^{-5}$

^a Units of keV.

^b Units of $\text{cm}^{-5} \text{ arcmin}^{-2}$ for the thermal components, and photons $\text{keV}^{-1} \text{ cm}^{-2} \text{ s}^{-1} \text{ arcmin}^{-2}$ at 1 keV for the power-law components.

MACS J0717.5+3745, rather than having traversed the cluster from the NW to the SE. This interpretation is further supported by the fact that the position of the X-ray peak is consistent with those of the cD galaxy and of the AGN hosted by the galaxy, as seen in Figure 1.

We measured the temperature and the brightness of the group by extracting spectra within $r_{2500} \approx 300 \text{ kpc}$ (Medezinski et al. 2013). The circular region, shown in Figure 2, had the center fixed at RA = $07^{\text{h}} 17^{\text{m}} 53.347^{\text{s}}$, Dec = $+37^\circ 42' 09.25''$. We assumed a group metallicity of 0.2 solar. The best-fitting parameters are summarized in Table 1. The normalization is equivalent to a luminosity of $(1.1 \pm 0.1) \times 10^{43} \text{ erg s}^{-1}$ in the energy band 0.1–2.4 keV. Based on the luminosity-mass scaling relations for galaxy groups (e.g., Connor et al. 2014), the group’s luminosity corresponds to $M_{2500} \approx 7 \times 10^{13} M_\odot$. Using optical data, Medezinski et al. (2013) determined $M_{2500} = (7.4 \pm 3.0) \times 10^{13} M_\odot$, which is consistent with our estimate.

4. X-RAY EMISSION FROM THE FILAMENT

To define the region of the filament that is least contaminated by ICM emission, we examined the surface brightness profile in a rectangular region aligned with the filament. In this region, the surface brightness decreases away from the cluster center, and then increases again approaching the SE group located along the filament; there is no radial range in this region where the surface brightness is flat. This suggests that the ICM of MACS J0717.5+3745 contaminates the filament, and this contamination needs to be considered when modeling the filament emission. Alternatively, the intrinsic brightness of the filament would be decreasing towards the group; however, evidence for this scenario is weak, especially given that faint ICM emission is seen SW of the filament.

We modeled the filament and the contamination from the ICM by extracting spectra in two rectangular regions:

⁴ <http://www.swift.ac.uk/analysis/nhtot/index.php>

⁵ Running this notebook requires the [bash_kernel](#) package.

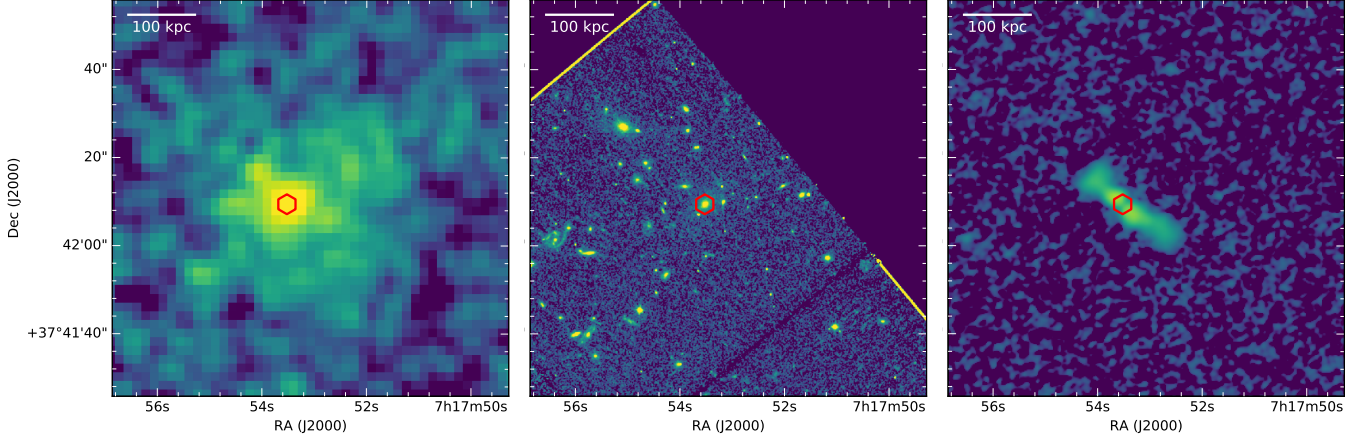


Figure 1. *Chandra* (left), *HST* (middle), and *VLA* (right) images of the region occupied by the galaxy group in the filament. The red hexagon marks the position of the group’s centrally dominating galaxy. The position of the BCG coincides with those of the radio AGN and of the X-ray peak.

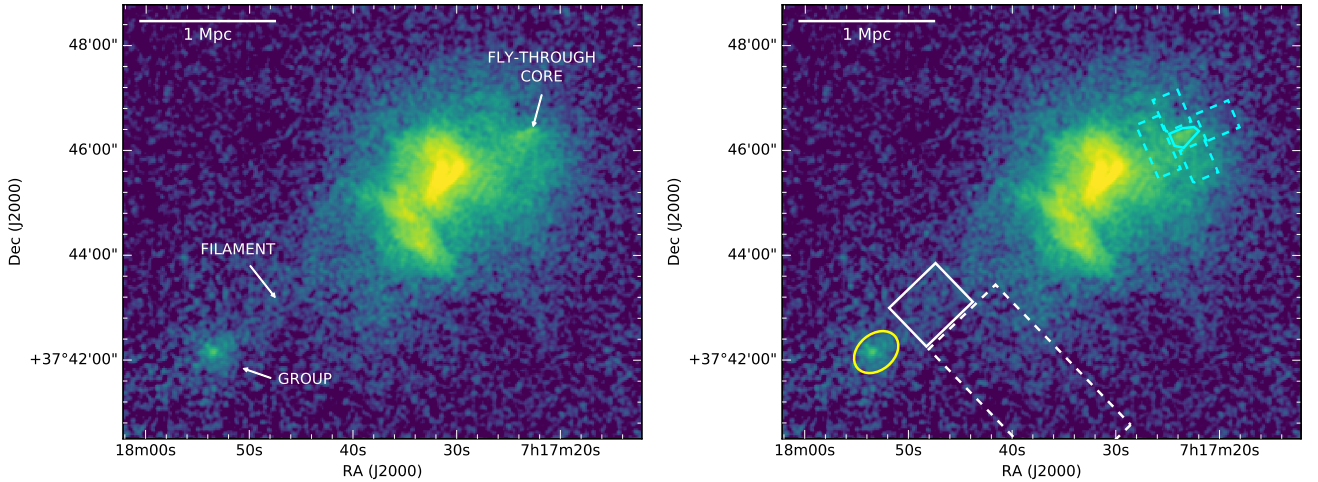


Figure 2. *Left:* Chandra 0.5 – 4 keV surface brightness map of MACS J0717.5+3745, showing the features discussed in this work. The image was exposure- and vignetting-corrected. Point sources were subtracted and the gaps were filled by sampling the regions surrounding the point sources. The gaps were filled to create a more visually appealing figure. However, the imaging analysis was done on images that did not have the gaps filled. The images used in the analysis are available online as supporting material. *Right:* Regions used in the spectral analysis. The regions of main interest are drawn in solid lines, while the regions used to characterize the contaminating/surrounding emission are drawn in dashed lines. The best-fitting parameters obtained for the gas in these regions are listed in Table 1.

one centered on the filament, and one positioned to the SW of it; NE of the filament, the signal-to-noise is too low for any meaningful information to be extracted from the spectrum. These regions are shown in Figure 2. The regions were chosen to avoid the bright parts of the ICM, as well as emission from the SE galaxy group. The emission in the SW region was modeled with a single thermal component, while the emission in the filament region was modeled with two thermal components—one describing ICM contamination, whose parameters were linked to those of the thermal component used to describe the SW region, and one describing emission from the filament. The spectra from the two regions were fitted simultaneously. Table 1 lists the best-fitting parameters obtained for a gas metallicity of 0.2 solar. Typical metallicities of cosmic filaments are still an open question, and it is plausible that they are lower than the typical metallicities in the outskirts of galaxy clusters ($\sim 0.2 - 0.3$; e.g. Simionescu et al. 2015). In this case, varying the metallicity causes only minor changes to the best-fitting pa-

rameters, well within the statistical uncertainty ranges. In one of the JUPYTER notebooks supporting this letter, we also list the results obtained for metallicities of 0 and 0.1 solar.⁶

The XSPEC normalizations of the thermal components listed in Table 1 are defined as

$$\mathcal{N} = \frac{n_e n_H V}{10^{14} 4\pi S_{\text{reg}} D_A^2 (1+z)^2}, \quad (1)$$

where we assume the density to be constant in each region, where n_e is the electron number density, n_H is the hydrogen number density, V is the volume of the region, S_{reg} is the projected area of the region, D_A is the angular size distance to the cluster, and z is the cluster redshift.

To calculate the density of the filament in the region shown in Figure 2, we assumed that in 3D the region is a parallelepiped with two rectangular faces perpendicular to the line of sight, and two rectangular and two par-

⁶ <https://goo.gl/e8xQD0>

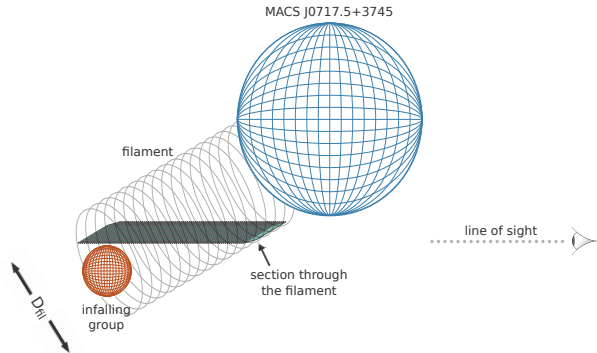


Figure 3. Sketch illustrating the geometry assumed for the large scale filament. The results vary insignificantly (compared to our other uncertainties) when assuming a parallelepiped geometry instead of a more natural cylindrical shape. For simplicity, we therefore used a parallelepiped for our volume estimate. The parallelepiped has two rectangular faces perpendicular to the line of sight, and two rectangular and two parallelogram faces parallel to the line of sight. The normal to the parallelogram faces points perpendicular to the page.

allelogram faces parallel to the line of sight. A sketch of this 3D section through the filament is shown in Figure 3. Jauzac et al. (2012), citing Ebeling et al., in prep., quoted a filament inclination angle $\theta \sim 75$ degrees with respect to the plane of the sky (the results below are highly sensitive to the uncertainty on the inclination angle). They also determined the filament has a diameter $D_{\text{fil}} \sim 3$ Mpc at the radius from which our spectra were extracted. Therefore, the volume of the parallelepiped corresponding to our region equals the filament diameter times the area of the parallelepiped face seen along the line of sight, i.e.

$$V \equiv V_{\text{ppp}} = D_{\text{fil}} S_{\text{reg}} / \cos \theta, \quad (2)$$

The projected region has a length of 1.2 arcmin (≈ 460 kpc) and a width of 1 arcmin (≈ 380 kpc), therefore $S_{\text{reg}} = 1.2 \text{ arcmin}^2$. Assuming $n_e = 1.2 n_H$ (e.g., Böhringer & Werner 2010), and finally substituting Eq. 2 in Eq. 1, the electron number density in the X-ray bright part of the filament is $\sim 2 \times 10^{-4} \text{ cm}^{-3}$. The critical density of the Universe at the redshift of MACS J0717.5+3745 is $1.7 \times 10^{-29} \text{ g cm}^{-3}$. Assuming the total baryon density is 4.4% the critical density of the Universe (Kirkman et al. 2003), the filament is overdense by a factor of ~ 450 compared to the mean baryon density of the Universe. Assuming a baryon mass fraction of 0.15 (e.g., Mantz et al. 2014), the mass density of the filament is $\sim 3 \times 10^{13} \text{ M}_{\odot} \text{ Mpc}^{-3}$. The filament density is therefore in excellent agreement with the density calculated from the weak lensing data by Jauzac et al. (2012) for the same filament geometry. The filament density corresponds to an overdensity of $\sim 100 - 150$ relative to the critical density of the Universe.⁷ The X-ray emission from the brightest part of the filament could originate from the hottest gas phase of the WHIM. Its density and temperature are consistent with reports of WHIM X-ray detection from other cluster filaments (e.g., Werner et al. 2008; Eckert et al. 2015). Alternatively, at least part of

the X-ray emission could be due to gas stripped from substructure that fell onto the cluster along the large-scale filament.

For the densities calculated above, the mass of the filament in the region from which the spectra were extracted is $\sim 6 \times 10^{13} \text{ M}_{\odot}$, with $\sim 9 \times 10^{12} \text{ M}_{\odot}$ in the hot gas.

In Figure 4, we show the surface brightness profiles in four sectors centered on the galaxy group seen within the filament. The surface brightness of the group becomes negligible beyond 1 arcmin. Between 1 and 2 arcmin, the profiles show the NW sector being significantly brighter than the other three; this sector covers the part of the filament between the group and the cluster. On the other side of the group, in the SE sector, the surface brightness between 1 and 2 arcmin is also larger than in the directions perpendicular to the filament. The SE sector includes part of the filament at higher cluster-centric radii. The surface brightness here is about half of that in the NW sector, which implies a baryon density lower by a factor of ~ 1.5 compared to the part of the filament closer to the cluster if the diameter of the filament is the same on both sides of the group. However, Jauzac et al. (2012) found that the diameter of the filament might be decreasing by a factor of up to ~ 2 from the region ahead of the group to the region beyond the group. Bearing in mind that the measurements of Jauzac et al. (2012) are highly uncertain, the decrease in diameter could account for the difference in surface brightness with no decrease in the baryon density of the filament.

The calculations made above can be found in one of the supporting JUPYTER notebooks accompanying this paper.⁸

5. SUMMARY

MACS J0717.5+3745 ($z = 0.546$) is a massive galaxy cluster selected as one of the six Frontier Fields targets. The cluster is the most morphologically complex merger, being the site of collisions between at least four subclusters. SE of the cluster, there is a large-scale cosmic filament that was first reported by Ebeling et al. (2004). Some of the subclusters involved in the merger have likely traveled along this filament before colliding with the previously existing structure. Jauzac et al. (2012) determined from optical data that the filament is ~ 19 Mpc long. The part of the filament that is near the cluster is visible at X-ray wavelengths. So far, the thermodynamic properties of large-scale filaments have only been studied in a handful of merging clusters (Werner et al. 2008; Eckert et al. 2015; Bulbul et al. 2016). Here, we used deep *Chandra* observations of MACS J0717.5+3745 to study the properties of the large-scale filament extending SE of the cluster center, and those of the substructures along the filament. Below is a summary of our results:

- The filament has a temperature of $1.58^{+0.51}_{-0.25} \text{ keV}$ and a density of $\sim 10^{-4} \text{ cm}^{-3}$. These are consistent at the 90% confidence level with the properties of the other filaments studied in X-ray (Werner et al. 2008; Eckert et al. 2015; Bulbul et al. 2016).
- The filament is over-dense by a factor of $\sim 100 - 150$ compared to the critical density of the Universe at the cluster redshift.

⁷ Jauzac et al. (2012) calculate an overdensity of $206 \pm 46 \rho_{\text{crit}}$, about 65% higher than our value, but this appears to be a miscalculation; our filament mass density values are consistent.

⁸ <https://goo.gl/eQbTYd>

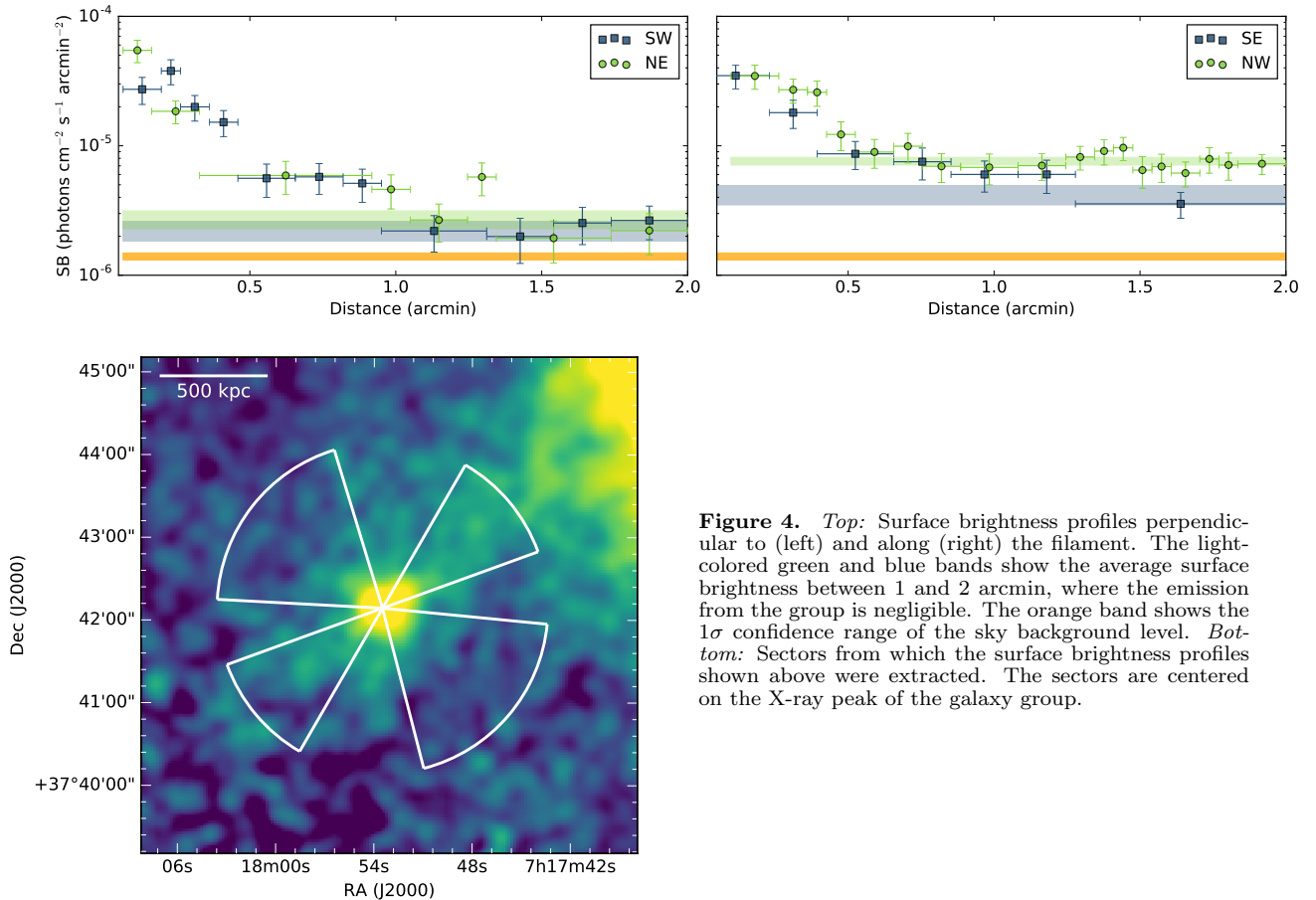


Figure 4. *Top:* Surface brightness profiles perpendicular to (left) and along (right) the filament. The light-colored green and blue bands show the average surface brightness between 1 and 2 arcmin, where the emission from the group is negligible. The orange band shows the 1σ confidence range of the sky background level. *Bottom:* Sectors from which the surface brightness profiles shown above were extracted. The sectors are centered on the X-ray peak of the galaxy group.

- The X-ray emission from the filament could be coming from the hottest and densest gas of the WHIM, or (at least partly) from gas stripped from substructures that fell into the cluster along the large-scale filament.
- The total mass contained in the X-ray-bright region of the filament is $\sim 6 \times 10^{13} M_{\odot}$, with $\sim 9 \times 10^{12} M_{\odot}$ in the hot gas.
- A little over 2 Mpc SE of the cluster center, embedded within the filament, there is a galaxy group with a temperature of ~ 3 keV and an X-ray luminosity of $\sim 10^{43}$ erg s $^{-1}$ in the energy band 0.1–2.4 keV. The mass of the group is estimated to be $\sim 7 \times 10^{13} M_{\odot}$. This group is likely approaching the cluster for the first time.

GAO acknowledges support by NASA through a Hubble Fellowship grant HST-HF2-51345.001-A awarded by the Space Telescope Science Institute, which is operated by the Association of Universities for Research in Astronomy, Incorporated, under NASA contract NAS5-26555. RJvW is supported by a Clay Fellowship awarded by the Harvard-Smithsonian Center for Astrophysics.

This research made use of APLPY, an open-source plotting package for PYTHON hosted at <http://aplpy.github.com>, and of ASTROPY, a community-developed

core PYTHON package for Astronomy (Astropy Collaboration et al. 2013). This research has also made use of NASA’s Astrophysics Data System, and of the cosmology calculator developed by N. Wright (Wright 2006). The *Chandra* data was obtained from the Chandra Data Archive, and analyzed using software provided by the Chandra X-ray Center (CXC) in the application packages CIAO and CHIPS. The surface brightness modeling used PYXEL, a PYTHON open-source modeling package for X-ray astronomy. The surface brightness profiles were plotted using MATPLOTLIB, a PYTHON library for publication quality graphics (Hunter 2007).

The optical data shown in the paper is based on observations made with the NASA/ESA Hubble Space Telescope, and obtained from the [Hubble Legacy Archive](#), which is a collaboration between the Space Telescope Science Institute (STScI/NASA), the Space Telescope European Coordinating Facility (ST-ECF/ESA) and the Canadian Astronomy Data Centre (CADC/NRC/CSA).

REFERENCES

- Astropy Collaboration, Robitaille, T. P., Tollerud, E. J., et al. 2013, *A&A*, 558, A33
- Böhringer, H., & Werner, N. 2010, *A&A Rev.*, 18, 127
- Bulbul, E., Randall, S. W., Bayliss, M., et al. 2016, *ApJ*, 818, 131
- Connor, T., Donahue, M., Sun, M., et al. 2014, *ApJ*, 794, 48
- Davé, R., Cen, R., Ostriker, J. P., et al. 2001, *ApJ*, 552, 473
- Dietrich, J. P., Schneider, P., Clowe, D., Romano-Díaz, E., & Kerp, J. 2005, *A&A*, 440, 453

- Ebeling, H., Barrett, E., & Donovan, D. 2004, *ApJ*, 609, L49
- Ebeling, H., Barrett, E., Donovan, D., et al. 2007, *ApJ*, 661, L33
- Ebeling, H., Edge, A. C., & Henry, J. P. 2001, *ApJ*, 553, 668
- Eckert, D., Jauzac, M., Shan, H., et al. 2015, *Nature*, 528, 105
- Einasto, M., Einasto, J., Tago, E., Dalton, G. B., & Andernach, H. 1994, *MNRAS*, 269, 301
- Elvis, M., Plummer, D., Schachter, J., & Fabbiano, G. 1992, *ApJS*, 80, 257
- Feldman, U. 1992, *Phys. Scr.*, 46, 202
- Hunter, J. D. 2007, *Computing In Science & Engineering*, 9, 90
- Jauzac, M., Jullo, E., Kneib, J.-P., et al. 2012, *MNRAS*, 426, 3369
- Kalberla, P. M. W., Burton, W. B., Hartmann, D., et al. 2005, *A&A*, 440, 775
- Kirkman, D., Tytler, D., Suzuki, N., O’Meara, J. M., & Lubin, D. 2003, *ApJS*, 149, 1
- Ma, C.-J., Ebeling, H., & Barrett, E. 2009, *ApJ*, 693, L56
- Mantz, A. B., Allen, S. W., Morris, R. G., et al. 2014, *MNRAS*, 440, 2077
- Markevitch, M., Gonzalez, A. H., David, L., et al. 2002, *ApJ*, 567, L27
- Mastropietro, C., & Burkert, A. 2008, *MNRAS*, 389, 967
- Medezinski, E., Umetsu, K., Nonino, M., et al. 2013, *ApJ*, 777, 43
- Simionescu, A., Werner, N., Urban, O., et al. 2015, *ApJ*, 811, L25
- Springel, V., & Farrar, G. R. 2007, *MNRAS*, 380, 911
- Springel, V., Frenk, C. S., & White, S. D. M. 2006, *Nature*, 440, 1137
- Umetsu, K., Zitrin, A., Gruen, D., et al. 2016, *ApJ*, 821, 116
- Umetsu, K., Medezinski, E., Nonino, M., et al. 2014, *ApJ*, 795, 163
- Werner, N., Finoguenov, A., Kaastra, J. S., et al. 2008, *A&A*, 482, L29
- Willingale, R., Starling, R. L. C., Beardmore, A. P., Tanvir, N. R., & O’Brien, P. T. 2013, *MNRAS*, 431, 394
- Wright, E. L. 2006, *PASP*, 118, 1711
- Zitrin, A., Broadhurst, T., Rephaeli, Y., & Sadeh, S. 2009, *ApJ*, 707, L102